International Forum on Aeroelasticity and Structural Dynamics
IFASD 2017
25-28 June 2017 Como, Italy

STUDY OF THE NONLINEARITY IN THE AEROELASTIC RESPONSE AT HIGH ANGLE OF ATTACK BY WIND TUNNEL TESTS ON THE ACTIVE AEROELASTIC TEST BENCH

Julien Ertveldt[1], Alfredo Lamberti[2], Ben De Pauw[3], Ali Rezayat[4], Rik Pintelon[5], Steve Vanlanduit[6]

[1]Vrije Universiteit Brussel (VUB)
Dept. MECH, Pleinlaan 2, B-1050 Brussels, Belgium
julien.ertveldt@vub.ac.be

[2]Universiteit Gent, Dept. MATCH,
Technologiepark Zwijnaarde 903, B-9052 Zwijnaarde, Belgium

[3]Vrije Universiteit Brussel, Dept. B-Phot

[4]Vrije Universiteit Brussel, Dept. MECH

[5]Vrije Universiteit Brussel, Dept. ELEC

[6]Universiteit Antwerpen, Dept. Op3Mech
Groenenborgerlaan 171, B-2020 Antwerp, Belgium

Keywords: nonlinear, high angle of attack, stall, wind tunnel

Abstract: The dynamic response of a cantilever wing at small and large angles of attack was tested using the Active Aeroelastic Test Bench (AATB) in the wind tunnel at low wind velocity (8 m/s, Re $\approx 120,000$). The compliant wing was excited at the root of the wing with a small 2° pitch angle. Advantage was taken from the fact that the AATB allows for arbitrary excitation of the wing in pitch and plunge at its constrained root. This property is exploited in order to excite the wing with an odd random phase multisine. The response of the instrumented wing was recorded by using both fibre Bragg grating (FBG) optical strain gauges and piezoelectric accelerometers. Using the spectral properties of the applied odd random phase multisine, the level of stochastic nonlinear distortions and the Best Linear Approximation (BLA) of the FRF was estimated for different angles of attack. A clear increase of the level of stochastic nonlinearities was observed when increasing the angle of attack up to 17.5°. These distortions were mainly focussed around the resonance frequencies and in the very low frequency range. This latter could only be observed in the measurements of the FBG strain gauges due to the high pass filter effect of the piezoelectric accelerometers. Comparison of the identified BLA with gust response measurements showed that in general good predictions from the BLA model were possible when the Signal to Distortion Ratio (SDR) was above 10 dB. For the tested wing this was for angles of up to 12°. Above this angle all resonance frequencies were still well approximated both in frequency and amplitude, however, a very important low frequency contribution was missing from the predicted data.

1 INTRODUCTION

The purpose of this article is to demonstrate a methodology that can be used for both the quantification and qualification of the dynamic nonlinear aeroelastic response of a wing under realistic, turbulence-like excitation at low and high angle of attack. In this paper we will identify the Best Linear Approximation (BLA) of the measured spectra that are distorted by nonlinearities of a certain level, depending on the set static offset angle of attack. It is not the goal of this work to extract a nonlinear model, but to study the influence of the nonlinearities on the linearised response, and this with an estimate of the level of the nonlinearities that are present. Hence, providing a framework to ease the decision for opting for a nonlinear modelling approach vs. a linear one on a rational basis.

The outline of this paper is as follows. Firstly the problem of nonlinear behaviour in the measurement of the Frequency Response Function (FRF) is described. Secondly, the Best Linear Approximation framework for nonlinear systems with a periodic input - periodic output relation is described. After this introductory discussion, the Active Aeroelastic Test Bench is introduced as the tool that allows to apply the desired excitation signals to a cantilever wing in the wind tunnel. Next, the results at both small and large angle of attack are discussed. Finally, the identified BLA models are used to predict the gust response of the wing, and comparison is made to the measured gust response.

There exists many possible sources that can result in the nonlinear behaviour of an oscillating cantilever wing. It is well known that in the linear regime of the lift curve slope, for an increasing angle of attack, the load on the wing increases. Hence, more deformation of the wing is likely to occur. Which can exploit the stiffening or weakening effect of the wing structure. Beside the possible structural nonlinear behaviour, approaching the stall angle will clearly introduce large aerodynamic nonlinear contributions to the dynamic behaviour of the wing [1]. Additionally, each of these physical reasons will result in distortion of the measured FRFs in a different manner, depending on whether one is dealing with a static weakening or stiffening effect of a given order, or a dynamic hysteresis effect for example. In reality it is very likely for an aeroelastician to be confronted with a combination of several of these sources of nonlinearity. One of the most important causes is of course the (dynamic) stall effect at large angles of attack. Due to the possible combination of nonlinear sources, the localisation and quantification of these is very difficult. The actual nonlinear modelling of these effects is even more difficult. Therefore, this paper focusses on applying well known and relatively easy to understand properties from a linear framework to the measurement of nonlinear aeroelastic responses of the cantilever wing.

By applying the correct excitation signals to the cantilever wing, it is these days possible to distinguish nonlinear behaviour from noise contributions for example. As it will be illustrated, although both can have a resembling appearance, there effect could be dramatically different. In order to illustrate the effect of nonlinearities in the measured response, one can imagine a simple static nonlinear system: $y(t) = u(t) + u^2(t) + u^3(t)$, excited by a sine at f_0. Due to the presence of a nonlinear quadratic stiffness term $u^2(t)$, one will not only observe a response at f_0 due to the linear part $u(t)$, but also at $2 \times f_0$. This is graphically illustrated by the red dot in the theoretical spectrum shown in Figure 1. Analogous, the cubic term in the system creates a contribution at f_0 as well as $3f_0$ (blue dots). If we now replace the static system by a linear mass spring damper system as often used for representing the vibrations of a cantilever wing, and adding a nonlinear quadratic stiffness term, one obtains:

$$m\frac{d^2y(t)}{dt^2} + c\frac{dy(t)}{dt} + k(1 + \alpha y^2(t))y(t) = u(t) \tag{1}$$

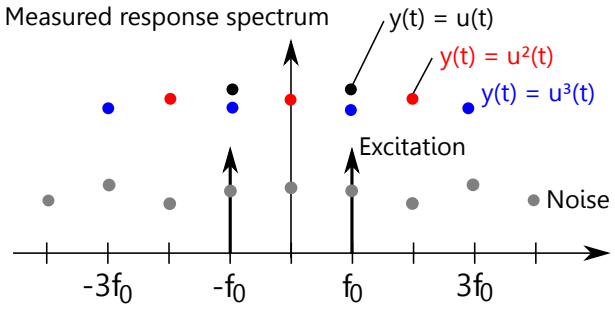

Figure 1: The response of a static nonlinear system $y(t) = u(t) + u^2(t) + u^3(t)$ will show combinations of the excited base frequency f_0.

The system in Eq. 1 is excited by random white noise in the frequency band from zero to 500 Hz, excluding DC. The resulting spectra is shown in Figure 2 (left).

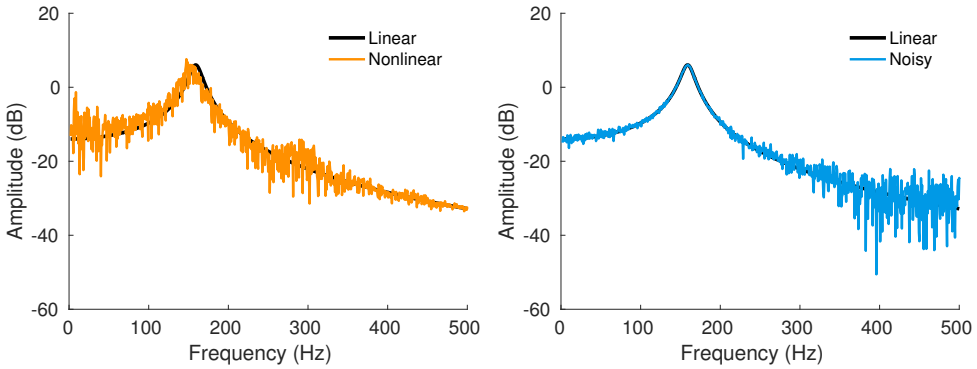

Figure 2: The spectrum of a noise corrupted linear system (right), and system with nonlinear distortions (left) are both *noisy*.

It is important to notice that, where the SNR is much higher for the linear response corrupted by uncorrelated white noise (right), this is not the case for the nonlinear noiseless response (left). Even more important is the fact that the response of the nonlinear system is different in terms of the resonance frequency and the amplitude at this frequency. The nonlinearity introduces a bias in the measured spectrum such that it does not coincide any more with the underlying linear part of the system. It is this property that makes it meaningful to define the Best Linear Approximation (BLA) of a nonlinear system for a given excitation spectrum (frequency content and amplitude). Hence, one will not obtain the true underlying linear model, but the linear model that matches best the nonlinear data.

As we illustrated in this section, using traditional (white noise, sweep, ...) excitation, distinguishing nonlinear behaviour from large noise contributions is not always easy. This is definitely true if both occur, such as during wind tunnel or in-flight testing. However, by applying the right excitation signals, such as odd random phase multisine signals, one can distinguish nonlinear distortions from noise contributions. This implicitly requires a wind tunnel test setup that allows to apply a measurable random phase multisine excitation signal to the wing without disturbing the aeroelastic behaviour of the wing. The AATB was build at the VUB in order to be able to excite a cantilever wing by such multisine signals with relative high frequency content without introducing wing-shaker interactions. The word *Active* in the name of the AATB stands

for the fact that the setup uses linear actuators for supporting the wing, which allows to inject energy into the system without disturbing the airflow around the wing.

An alternative option could be to use control surface (CS) excitation following a similar odd random phase multisine motion profile. However, due to the complexity of the aerodynamic flow around a deflecting control surface combined with the lack of the possibility to directly measure the resulting forces upon the CS deflection, excitation of the wing at the root is preferred in order to obtain a (more) linear relation between applied excitation signal and resulting excitation forces. It is explained in [2] that the excitation in position of a constrained wing at its root results in the same response as a (scaled) force near the clamped root.

A multisine is, as the name suggests, a signal that consists of the sum of different sines with harmonically related frequencies.

$$r(t) = \sum_{k=1}^{F} U_k \sin\left(2\pi k f_0 t + \phi_k\right) \tag{2}$$

with U_k the deterministic amplitude spectrum, $f_0 = 1/T$ the base frequency, with T the length in time of one period, and ϕ_k the phase for each excited frequency line k in the set of F excited frequencies.

If the phases ϕ_k are chosen as random values over the set of excited frequencies k, such that $E\{e^{j\phi_k}\} = 0$, with $E\{\bullet\}$ the expected value, then we speak of a random phase multisine. A good reason for doing this is to avoid the onset of all of the sines at the start of the composed signal, which would result in a large spike and thus crest factor. Another, perhaps even more important reason is the robustness towards nonlinear distortions that random signals offer [7].

Because a multisine is a periodic signal it can easily be repeated for multiple periods without introducing leakage errors. Additionally, by selecting the excited frequencies deterministically, when adding periods, the same frequencies will still remain excited. Hence, by doing a measurement where the total number of samples $N = P \times N_{pp}$ is the product of the number of periods P and the number of samples in each period N_{pp} an excitation spectrum is created where in between two excited lines one can find $P - 1$ non-excited lines. It will be shown later on that this is a very useful property for estimating noise levels, because noise also contributes at the non-excited lines. In Figure 3 the amplitude spectrum of one period of a full (i.e. all lines excited in the band 0.8-50 Hz) random phase multisine is illustrated (left). Followed by the resulting spectrum when concatenating the signal to eight periods (right).

Using multiple periods and realisations of an odd random phase multisine, one can take advantage from the fact that nonlinear distortions in an NL - Periodic Input Same Periodic Output (NL-PISPO) system are periodic, but noise contributions are random. Hence, averaging over different periods and realisations, one can make an estimate of the level of stochastic nonlinear distortions and the noise level in the measured input and output spectra [3–7]. The fundamentals of this method are illustrated in Figure 4 and can be summarised as follows. Performing M experiments with different random phase realisations $R_1, ...R_M$, of a periodic input signal of P periods, one obtains a set of input-output data $X = [Y, U]$. Averaging each experiment over the different periods and projecting the different phase realisations to the same reference phase,

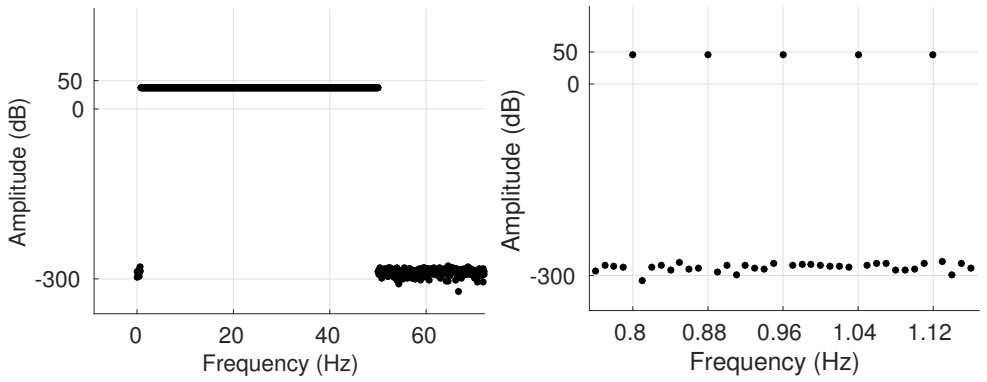

Figure 3: DFT spectrum for one (left) and eight (right) periods of a full random phase multisine exciting from 0.8 Hz to 50 Hz, illustrating the $P-1$ or seven, non-excited lines in between the excited for the multiple periods.

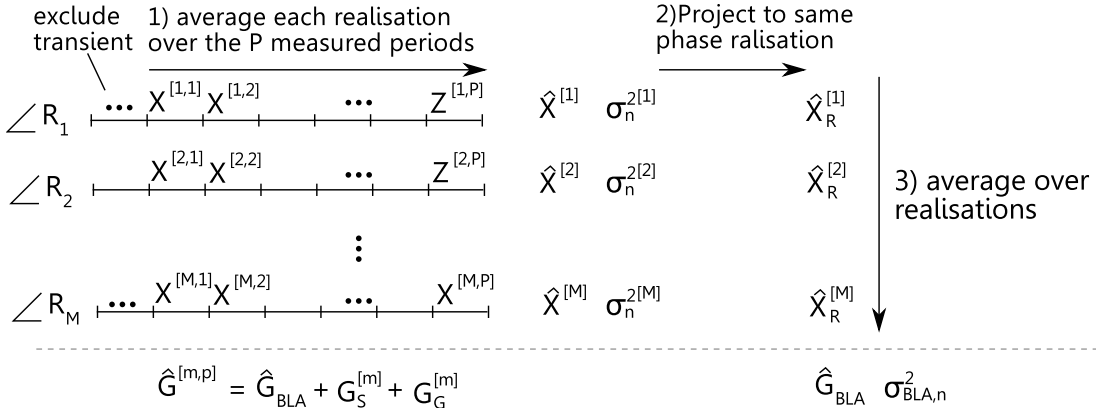

Figure 4: Averaging over the different periods and realisations of a set of random phase multisine experiments allows for the estimation of the BLA and the distinction between noise variance and the level of nonlinear distortions. $X = [Y, U]$.

one can finally average over the different realisations in order to obtain the BLA of the distorted spectra.

Many nonlinear systems behave as an NL-PISPO system [4]. This means, that the nonlinear system excited by a periodic signal will result in a periodic response. Examples are static nonlinear systems such as composite stiffening wings, but also dynamic hysteresis effects as in the case of very high pitch angle oscillations leading to dynamic stall. Although many more nonlinear effects can be captured in the NL-PISPO framework, one has to be aware that any possible bifurcation or chaotic problem can not be captured, and each BLA is linked to an excitation spectrum content and amplitude. Figure 5 illustrates what was previously mentioned. A NL-PISPO system can be represented by its BLA with an additional error source added to the output. This error source, behaving much like measurement noise, covers for the presence of the stochastic nonlinear distortions in the output of the nonlinear system, whereas the BLA takes into account the bias introduced with respect to the true underlying linear system.

In the sequel of this paper we will firstly describe the Active Aeroelastic Test Bench that was build in order to be able to excite a cantilever wing with the desired odd random phase multisines in order to extract the BLA at different test conditions.

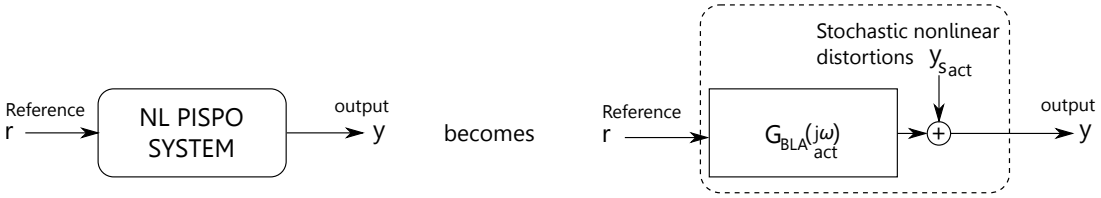

Figure 5: For a nonlinear system with a periodic response this NL-PISPO system can be replaced by its Best Linear Approximation and an additional error source: the stochastic nonlinear distortions.

2 THE ACTIVE AEROELASTIC TEST BENCH AND INSTRUMENTED CANTILEVER WING

The Active Aeroelastic Test Bench (Figure 6) was build around the low speed wind tunnel facility of the Vrije Universiteit Brussel. The wind tunnel test section measures 2 m $\times$ 1.4 m $\times$ (width $\times$ height) and a maximum velocity of 20 m/s can be obtained in the test section. The tunnel can only be operated at atmospheric conditions close to sea level. The goal of this setup was to obtain a test platform for the study of the dynamic aeroelastic behaviour of a (cantilever) wing. This for both the study of unsteady aerodynamic, as well as, aeroelastic behaviour. Figure 7 illustrates the experiments in different areas of expertise that all can be performed on the AATB. Unsteady aerodynamic experiments with a rigid wing of which the position was controlled at both extremities were conducted previously on the AATB and have been reported in [8, 9]. In this proceeding, preliminary results of aeroelastic experiments using a compliant cantilever wing at high angles of attack are discussed. In order to identify the behaviour of this wing as a dynamic system for either unsteady aerodynamic or aeroelastic experiments, accurate, controllable and measurable excitations needed to be applied to the wing.

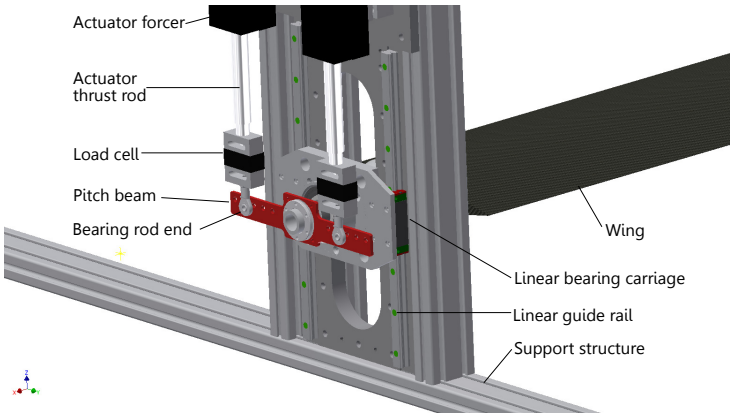

Figure 6: The AATB uses a pitch and plunge mechanism with linear and rotary bearings and linear motors.

The aeroelastic experiments discussed in this paper were performed using a cantilever wing build from DOW ® FLOORMATE ™200 extruded polystyrene foam (XPS) with density of 30 kg/m^3 and a Young's modulus of 10 MPa. This foam was CNC cut into a NACA 0018 shape with chord of 22 cm and span of 1.2 m. The foam core was then manually coated with an epoxy resin layer of approximately 0.8 mm, and sanded to a smooth surface to provide an adherent surface for the installation of the optical FBG strain gauges and accelerometers. The location of these sensors are indicated in Figure 8. The total mass of the wing is approximately 250 g. Hence, a very lightweight but also compliant wing was tested.

In the next Section we will discuss the necessity of an accurate control over the excitation of the wing is such important in order to obtain information about the level of nonlinearity in the

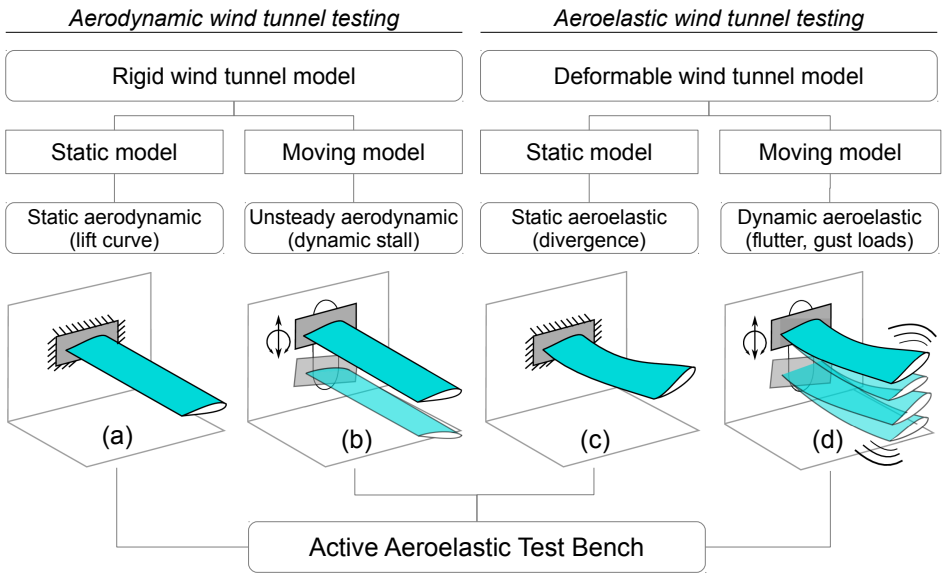

Figure 7: Schematic overview of the different types of experiments that are possible on the AATB, depending on wheter a rigid or deformable wind tunnel model is used, and the model is excited at the root or not.

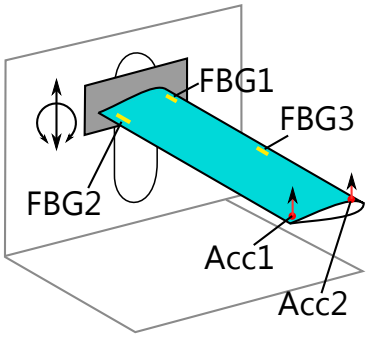

Figure 8: Three FBG optical strain gauges and two accelerometers are mounted on the cantilever wing.

aeroelastic response.

3 THE LEVEL OF NONLINEARITY IN THE MEASURED RESPONSE WITH INCREASING ANGLE OF ATTACK

3.1 Quantification of the level of nonlinearity at zero angle of attack

The goal of this paper is not to identify a nonlinear model of the aeroelastic vibrations. Instead, the goal is to estimate different linear approximations for each condition. We estimate a linear approximation for each setpoint in the nonlinear regime, but this by taking into account the effect of the distortions introduced by the nonlinearities onto the measured output spectra and FRF.

As was already discussed in the introduction, the use of odd random phase multisine excitation signals allows to obtain the BLA of the system for that given excitation spectrum (frequency content and amplitude). Additionally, the wide band excitation leads to a high frequency resolution because few experiments are required. Hence, each experiment can have a reasonable long measurement time. On the other hand, a periodic repetition is required and multiple experiments are preferred for a robust analysis (see [5] for the details), reducing the frequency

resolution, but at the benefit of obtaining information about the level of the nonlinear distortions. In practice for the measurements discussed in this paper a set of 6 odd random phase multisine experiments were performed containing 8 periods, exciting for each experiment the same random chosen set of odd frequencies in the interval between 0 and 60 Hz, excluding 0 Hz. This results in a repetition of 6 measurements of 160 s (20 s per period) for each angle of attack. The resulting pitch angle excitation signals in both time and frequency domain are illustrated in Figure 9. Two important messages are to be remembered from this figure. Firstly, because the bandwidth of the position controller is limited to 8 Hz in the current AATB, a (phase) difference between the reference and commanded signal in the amplitude spectrum exists. However, because smaller pitch angles are required at higher frequencies (constant acceleration level), this is not an actual limitation for the performed experiments, and excitation frequencies of 60 Hz can easily be reached. Secondly, although the setup does not exactly track the reference signal, the desired separation between the excited and non-excited frequencies illustrates both a good signal to noise as well as signal to distortion ratio for the pitch angle command. The presence of a set of energy above the. However, because both reference and input signal are known, the output spectra were corrected for the presence of the small nonlinear distortions in the pitch excitation signal (see [5]). The presence of these nonlinearities of one order of magnitude smaller than the actual excitation level is not unexpected because of the use of a bearing mechanism to support the wing. However, because the excitation is a quantity (i.e. pitch angle) that can be directly measured, one can also compensate for this.

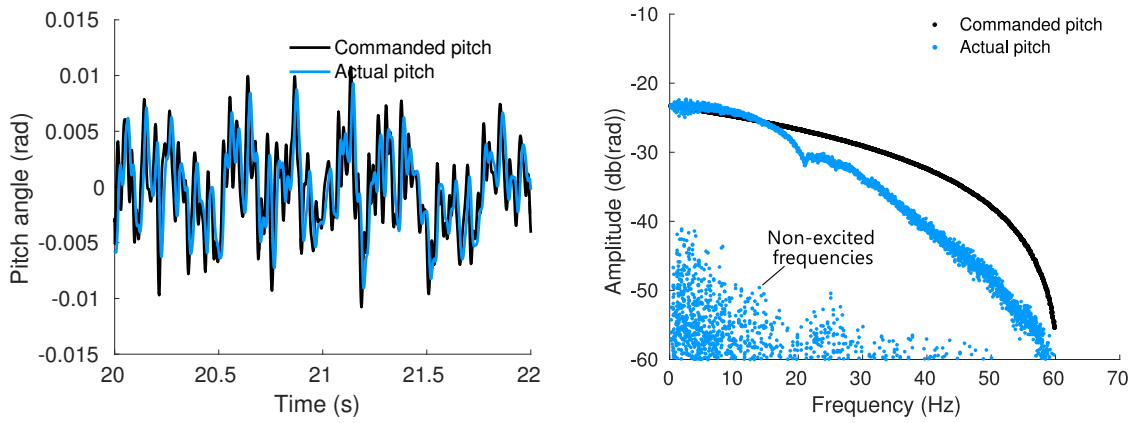

Figure 9: Reference (black) and actual pitch angle (blue) signal (left) and spectrum (right). The spectrum illustrates a good separation between excited and non-excited frequencies.

In order to provide a benchmark for analysing the results at high angle of attack we will first look at the level of nonlinear distortions observed in the output spectrum of the wing excited by an odd random phase multisine at wind-off conditions. In Figure 10 the BLA FRF is shown in black together with the level of nonlinear distortions (red +). The two additional lines are the total variance (blue) and the noise level (green). One can see that this latter is well below the level of the stochastic nonlinear distortions (red +), hence, even at wind-off conditions the level of the nonlinear distortions is more important than measurement noise. Although more important, the Signal to Distortion Ratio (SDR) is around -20 to -30 dB. These values are in the expected range for monolithic structures as was previously illustrated by [10].

Four wing resonance frequencies were excited in the band from 0 to 60 Hz, excluding the actual DC component. In the sequel of this paper the resonance frequencies and damping ratios extracted from the linear approximation provided by the BLA are compared to these for the higher angle of attack cases at a wind velocity of 8 m/s ($Re \approx 120{,}000$). A summary of the

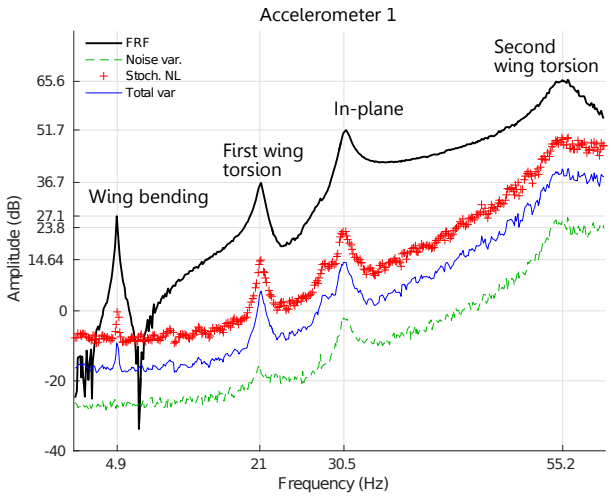

Figure 10: The acceleration FRF with its standard deviation and the level of stochastic nonlinear distortions.

first resonance frequencies of the wing measured at wind-off and 8 m/s are given in Table 1. One of the goals of the next Section will be to analyse the changes of these resonance frequencies and damping ratios observed for the increasing angles of attack.

Table 1: Resonance frequencies and damping ratios for the TW-01 at 8 m/s and wind-off conditions.
Accelerometer based

Mode	Wind-off		8 m/s 0° AOA	
	f_n $(3\sigma_{f_n})$ [Hz]	ξ_n $(3\sigma_{\xi_n})$ [%]	f_n $(3\sigma_{f_n})$ [Hz]	ξ_n $(3\sigma_{\xi_n})$ [%]
Wing bending	4.9 (0.003)	1.70 (0.05)	5.05 (0.047)	12.2 (1.02)
Wing torsion	21.1 (0.009)	1.65 (0.04)	21.1 (0.009)	2.03 (0.045)
Wing in-plane	30.6 (0.008)	1.57 (0.03)	31.04 (0.011)	2.73 (0.034)
Wing 2nd torsion	55.2 (0.054)	2.48 (0.10)	55.31 (0.054)	2.78 (0.11)

3.2 Influence of the angle of attack on the level of nonlinearity in the dynamic response

The same procedure as discussed in the previous subsection was subsequently repeated for data collected with an angle of attack at respectively 7.5°, 12° and 17.5°. Notice that because a multisine is exiting a wide frequency band in one experiment, each experiment can have relative high frequency resolution because few experiments are required in comparison with a stepped sine approach.

Figure 11 provides a comparison of the level of the stochastic nonlinearities (markers) and BLA (solid line) for different static offset angles of attack observed by the accelerometers at trailing (TE = Acc. 1) and leading edge (LE = Acc. 2). The first global impression from the figure is that the BLA FRFs (solid line) for the different static angles of attack are not so different one from the other. Only for the 17.5° angle of attack case we notice some major differences around 10 Hz. For the level of the stochastic nonlinear distortions we can see that an increase of around 15 to 20 dB occurs at low frequencies below 5 Hz. Bringing the level of the stochastic distortions even above the energy level of the linearised response.

It was mentioned in the previous paragraph that no large differences were observed when comparing the BLA FRFs for the different angles of attack. Specially once past the 10 Hz mark we

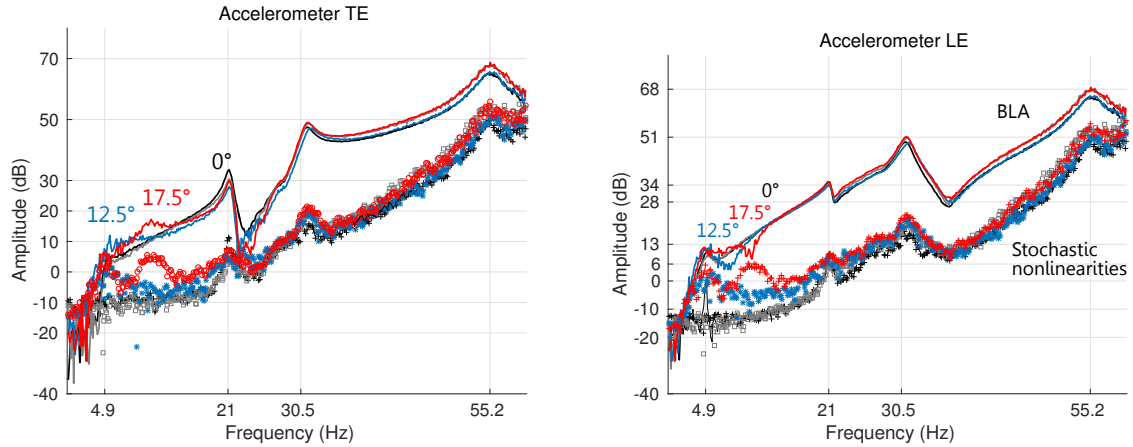

Figure 11: Comparison of the estimated BLA and level of stochastic nonlinear distortions at wind-off, 8 m/s and for different static angles of attack show that only for very large angles a significant change of the BLA and NL distortions for frequencies below 10 Hz.

observe very little changes. We remember the reader that the first wing bending frequency was around 5 Hz for the TW-01 wing. Figure 12 provides a comparison of the estimated damping ratios and resonance frequencies of the BLAs for the different angles of attack and vibration modes. The major conclusion to draw from these results is the fact that no change of the resonance frequency, neither the damping ratio of any of the modes other than the wing bending mode is visible. With respect to the first wing bending mode we can say that the resonance frequency (right plot) is only slowly changing until a very large angle of attack of 17.5° is obtained. Because of the low resolution w.r.t. the angle of attack we can not postulate whether this is a gentle or sudden increase. For the damping ratio (left plot), a much larger and also somehow smooth variation of the damping ratio is obtained. Both the damping ratio as well as its estimated standard deviation is increasing at least about a factor four. The increase in standard deviation is not un-expectable because of the increasing level of stochastic nonlinear distortions and hence total variation on the measurements, as because of the increased damping of this mode, suppressing its contribution to the measured response.

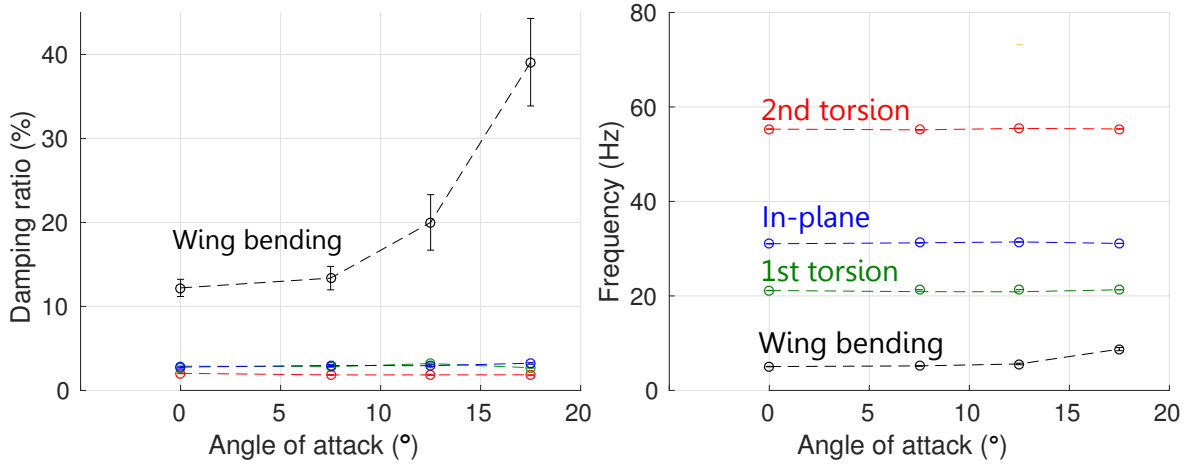

Figure 12: Based on the measured accelerations, only the first bending mode, which is highly damped, is affected by the increasing angle of attack using the accelerometer data.

Besides accelerometers, the TW-01 wing is also equipped with strain gauges. Because acceleration levels square quadratically with the amplitude of the vibration, low acceleration levels are measured at very low frequencies. Hence, using strain gauges, which are related directly to the

amplitude of the motion, are expected to acquire more information in the low frequency range, where large oscillations typically occur. Therefore, in Figure 13, a comparison is made of the BLAs and the level of the stochastic nonlinear distortions, in a similar manner to the results for the accelerometers presented in Figure 11.

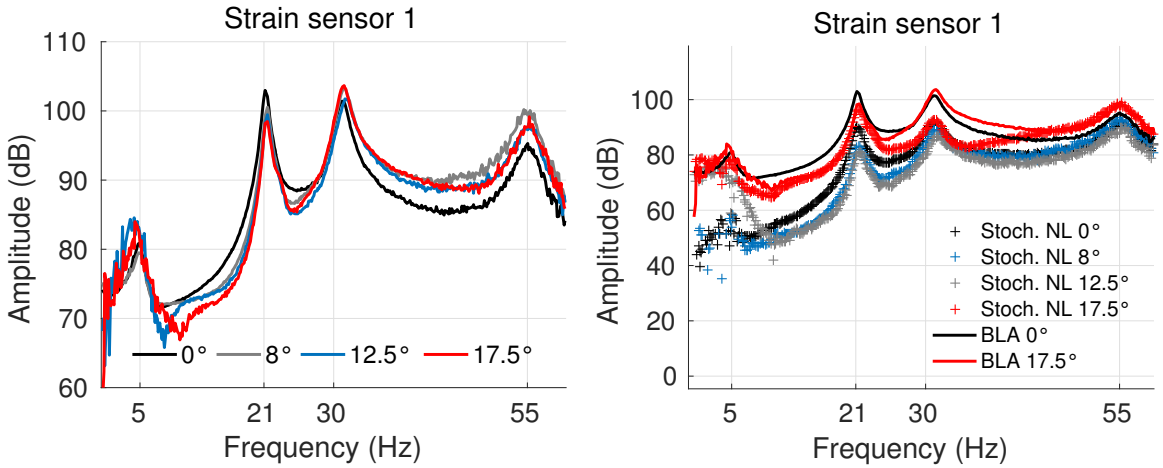

Figure 13: Limited global variation is observed between the BLA's at different angles of attack between 0° and 17.5° (left). The same is true for the level of stochastic nonlinearities (right). Both obtained from the FBG strain data.

Because the interpretation of small variations directly from the FRF on a graphical basis is not straightforward, the resulting changes in damping ratios and resonance frequencies extracted from the linearised BLA's are summarised in Figure 14. In this Figure one should notice that the results are less smooth than for the accelerometer data. No conclusion could be formulated based on only this instrumented wing. One has to remember however, that the level of the stochastic nonlinear distortions in the low frequency range is much more pronounced in the very low frequency range for the strain sensors, which could result in this larger variation. The global trend for the first wing bending mode is similar as the one observed for the accelerometer data. Even though there is a very large variance for the 17.5° angle, the difference is statistically significant.

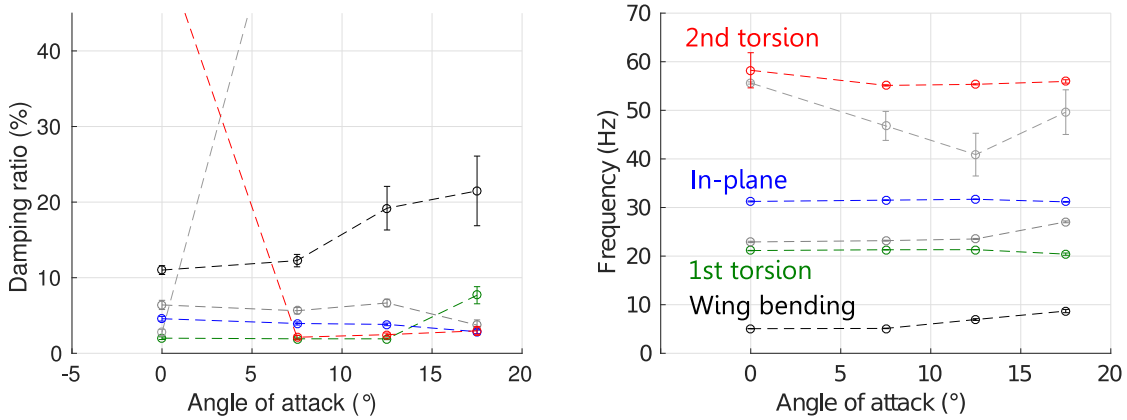

Figure 14: Variation of the damping ratios (left) and resonance frequencies (right) identified from the strain measurements at different angles of attack. Only the first wing bending shows significant variation, as was already observed for the acceleration in Figure 12.

In order to evaluate the usability of the estimated BLA models we will compare the predicted gust response extracted from the BLA models to the actual measured gust response.

4 EVALUATION OF THE ESTIMATED BLA THROUGH COMPARISON WITH GUST RESPONSE MEASUREMENTS

Before comparing the predicted gust response with the actual measured response, a summary of the approximations made in this analysis procedure is appropriate. First of all, the estimation of a BLA system assumes that the measured response of the wing is periodic. By repeating the gust response measurement multiple times we could validate this assumption and confirmed that we can treat the cantilever wing studied as a NL-PISPO system.

Figures 15 and 16 show respectively the measured time domain and frequency domain responses for the $1 - cos$ gust excitation at different angles of attack. The response measured by accelerometer 2 is shown on the left side in the figures, whereas the right side shows the recorded strain values. Because the gust experiments were repeated over ten periods, a grey set of the actual data is plot together with the mean value. One should notice a large difference between the accelerometer based and the strain gage based data. Where the strain gage data clearly shows a significant low frequency contribution for the larger angle of attack experiments, this is not visible for the accelerations. Secondly, although much less pronounced for the accelerometer data, both show an increase of the total standard deviation over the different periods, but all reasonably close to the mean values. Indicating that the level of nonlinearity also increased for the accelerometers, but because of the lack of sensitivity in the low frequency band, this is not clearly visible from the time domain data. Finally, the NL-PISPO (periodic input same periodic output) assumption is validated for both.

If one now also looks at the frequency domain representation (see Figure 16 of exactly the same data discussed in the previous figure, one can see that indeed the total standard deviation for the accelerometer also increased in a similar manner as for the strain data. With the major difference that the high pass filter effect of the piezo electronic accelerometers filters much of the response below 10 Hz. Replacing the piezo based sensors with MEMS accelerometers that have a frequency band starting from 0 Hz will probably result in similar data as obtained with the strain gauges.

Finally, to conclude this results section, a comparison is made between the predicted gust response from the BLA models and the actual measured gust response that was just discussed. Before presenting the actual results we want to emphasise that one has to remember that the BLA models are linear models that were build using odd random phase multisine signals with a different excitation spectrum and amplitude than the gust measurements. Hence, because the superposition or scaling principle does not hold for nonlinear systems, one should not expect a good agreement between both models. Figure 17 compares the predicted gust response from the BLA with the actual measured response. Again, both time domain and frequency domain data is shown. The first conclusion to draw from the time domain data is that there is a very poor agreement between the predicted (blue) and the measured response (black). However, in a second look, also including the predicted spectrum, one can notice that in fact many of the oscillations are still accurately predicted, but that a very low frequency contribution is being missed. Without a doubt, because of the large amplitude of this low frequency contribution, the linearised model as such is not usable for an accurate prediction of the gust response.

In order to better understand what is the actual cause for these very low frequency contributions that were already observed during the multisine experiments, some additional experiments were performed with a high-speed video camera filming the motion at the wing tip (Figure 18). Using markers glued on a lightweight beam that was attached to the wing, the motion in terms of

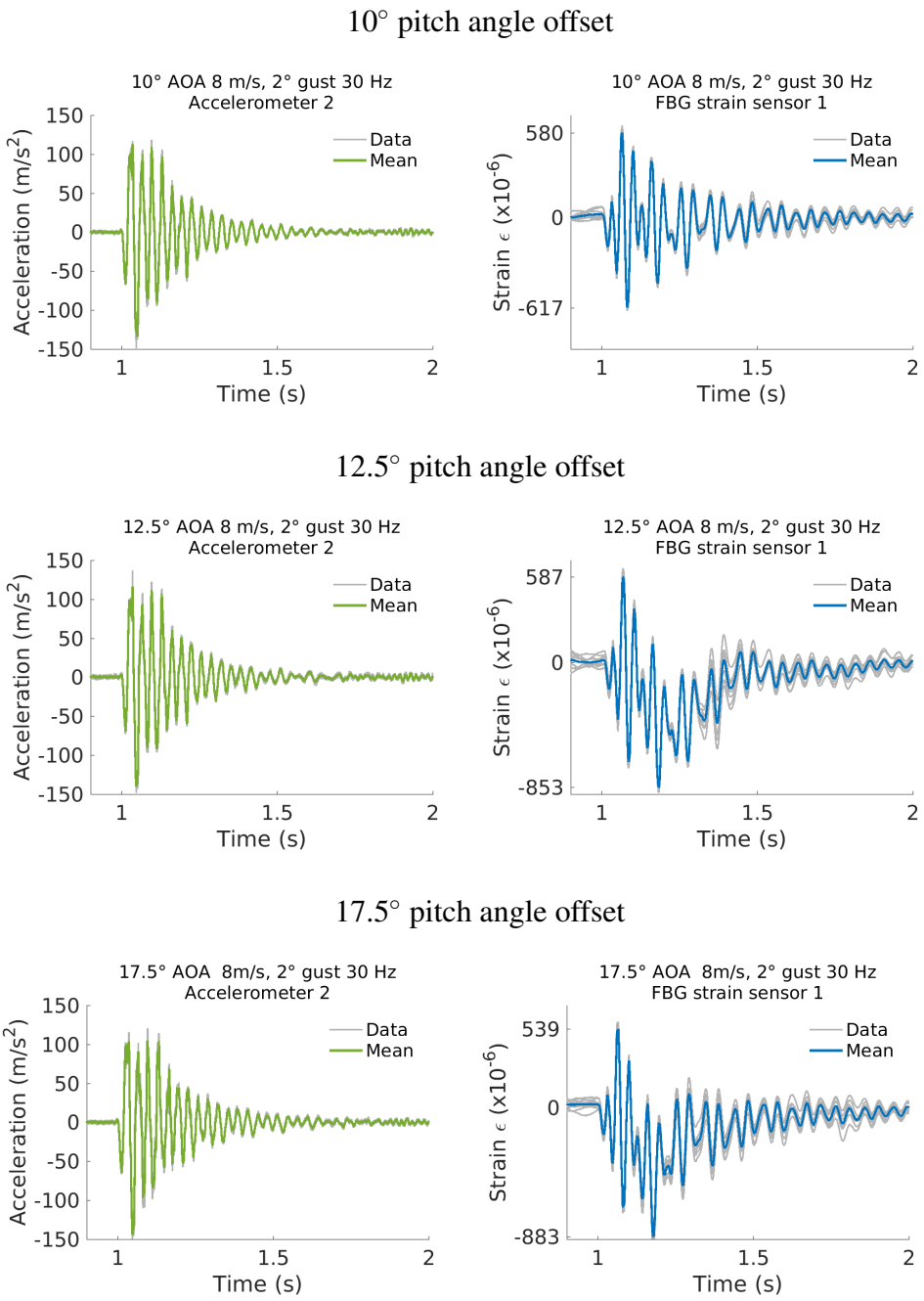

Figure 15: Measured output signals (grey) and averaged values (solid color) for the 0° static geometric angle of attack for the wind-off condition (top) and at 8 m/s (bottom).

pitch angle and vertical plunge motion of the wingtip could be recorded. The results of this analysis procedure is illustrated in Figure 19. Where three values are illustrated. The pitch angle (top), the plunge position (middle) and the in-plane motion (bottom). Different gust response experiments were performed, all about a 17° angle of attack, but with different pitch amplitude, ranging from 1 to 2.5°. One can notice that the response of the pitch angle of the wing shows no asymmetric low frequency contribution as we observed in the accelerometer and strain data, which is a combination of mainly torsion, bending and to less of an extend in-plane motion. The vertical displacement of the wing tip, indicated as the plunge motion, however, does show a large build in amplitude after two periods of oscillation at the wing torsion resonance frequency. A similar, but less pronounced trend is also visible for the in-plane motion. The most likely explanation for the observed behaviour could be related to the

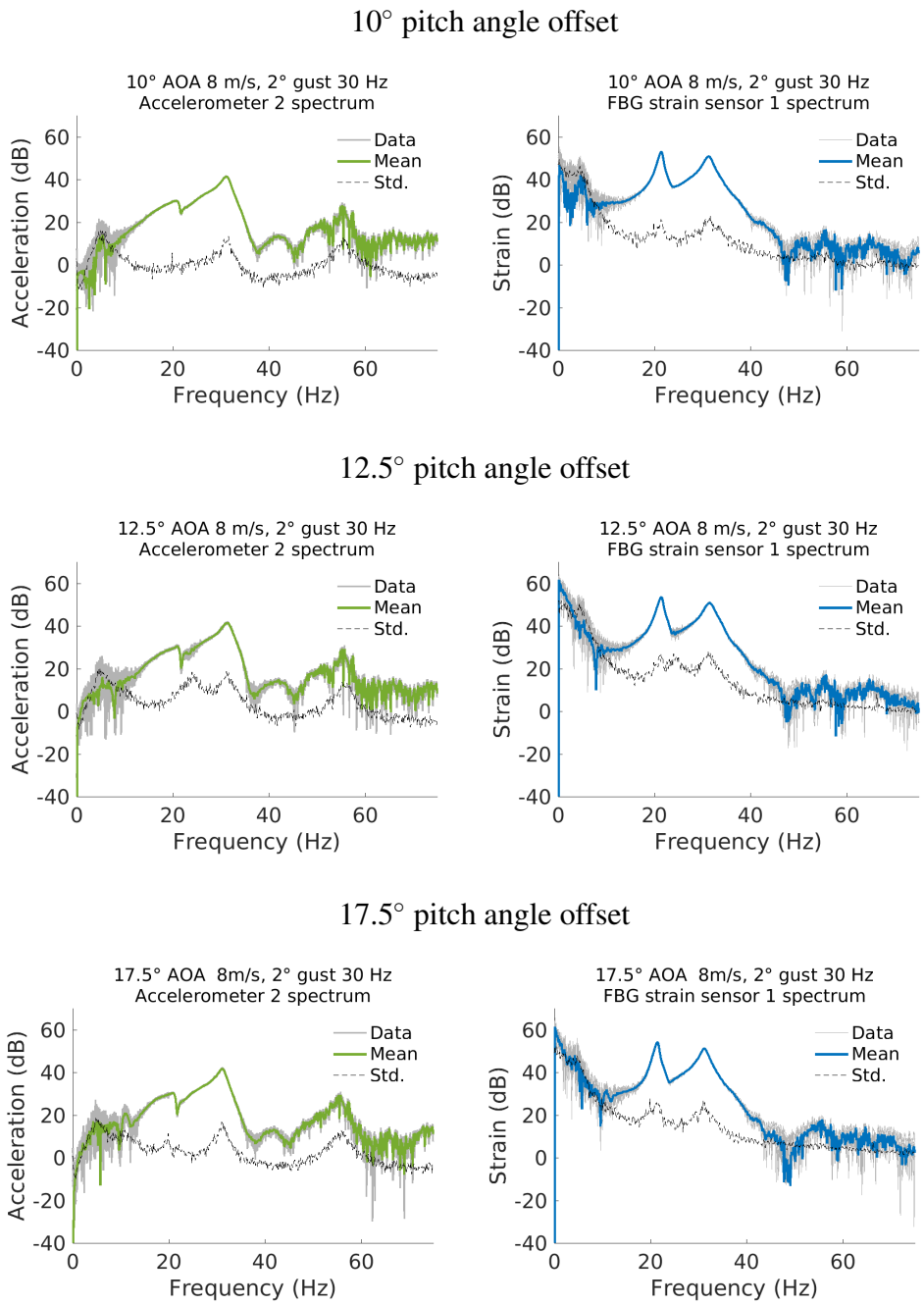

Figure 16: Measured output spectra (grey), averaged values (solid color) and standard deviation (dashed) for the 0° static geometric angle of attack for the wind-off condition (top) and at 8 m/s (bottom). .

presence of an isola in the nonlinear frequency-energy plot of the wing.

In order to analyse the actual source and behaviour of this dominating nonlinearity a further study of the behaviour of the wing for different excitation frequencies and amplitudes (energies) is required. Using the restoring force method as used in [11, 12] and based on single harmonic sine excitations one could identify the shape of this nonlinear behaviour in order to further characterise it. The main advantage is that by performing the multisine experiments at different conditions one can easily test in one experiment a complete frequency band for significant nonlinear behaviour. Hence, based on the identified BLA models discussed in this paper, further research can now be started using the defined frequency ranges, angles of attack, as well as pitch amplitude in order to identifying the actual nonlinear characteristics for the identified cases

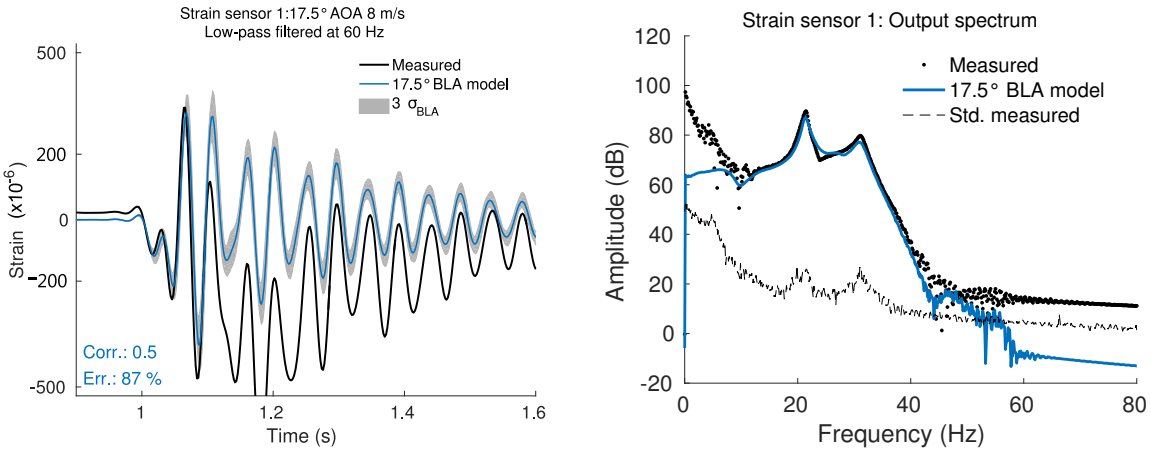

Figure 17: Prediction (blue) and actual measured (black) $1-cos$ gust response at an angle of attack of 17.5°. Time series (left) and measured output spectrum (right). The actual measured gust response illustrates an important low frequency content that is not captured with in the given standard deviation (grey shading) of the identified model.

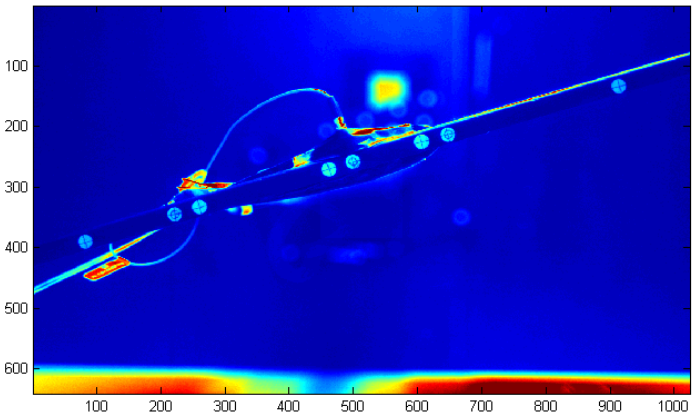

Figure 18: An example of an image captured by the high speed camera for tracking of the markers applied to a beam glued to the tip of the cantilever wing. The original image is in greyscale but transformed to colour for better visibility of the tracking markers in a printed copy.

requiring more attention.

5 CONCLUSION

Throughout this paper we firstly introduced the AATB wind tunnel test setup as a tool that allows to accurately excite a wing at its clamped root in pitch or plunge. Using excitation in position at the root of the wing allows to apply a measurable excitation signal. From comparing the level of the stochastic nonlinear distortions in both the measured output and input signals, one can estimate the level of stochastic nonlinearities introduced in the system.

It was shown that for reasonable levels of signals to nonlinear stochastic distortions SDR ¿ 10 dB, using an odd random phase multisine excitation for the identification of the BLA model allows for good approximation of the gust response, although that the content and amplitude of both input spectra differs. However, when the SDR approaches zero, the From the same analysis one could also that observe that even though the SDR is very low in certain frequency bands, prediction of the response in some of these low SDR bands was still possible, why for very

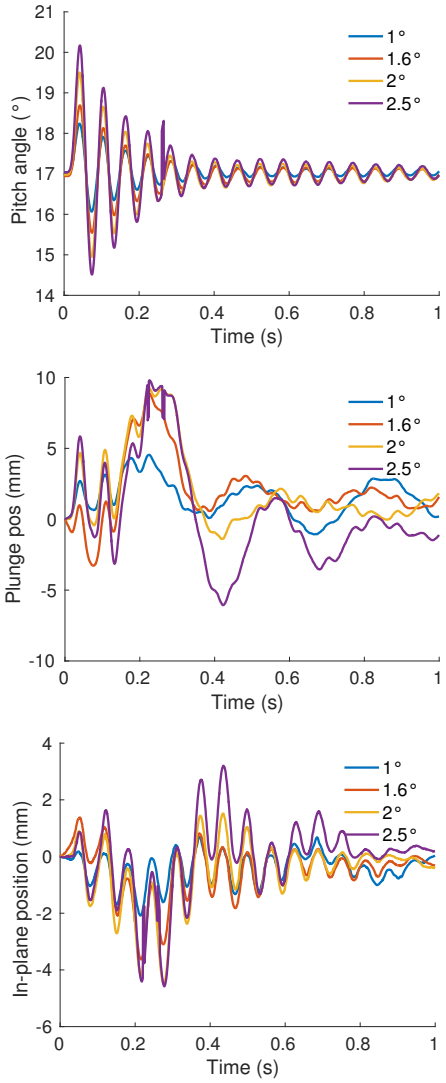

Figure 19: Measured pitch (top), plunge (midle) and in-plane displacement of the wing tip for pitch gust experiments with different pitch angle amplitudes. We notice a major difference in the frequency content of the plunge response, compared with the resembling pitch and in-plane deflection.

high level of the distortions at low frequencies, this was not possible. Hence, we can conclude that if SDR remains above 10 dB, a good approximation of the gust response of the wing was possible using a linear approximated model. However, for the very high angle of attack cases up to 17.5°, a significant very low frequency contribution was underestimated.

6 REFERENCES

[1] Dunn, P. and Dugundji, J. (1992). Nonlinear stall flutter and divergence analysis of cantilevered graphite/epoxy wings. *AIAA Journal*, 30(1), 153–162. ISSN 0001-1452. doi: 10.2514/3.10895.

[2] Ertveldt, J. (2017). *Application of frequency-domain system identification to wind tunnel experiments on the Active Aeroelastic Test Bench*. Phd thesis, Vrije Universiteit Brussel, Dept. MECH, Pleinlaan 2, B-1050 Brussels, Belgium.

[3] Vaes, M., Schoukens, J., Peeters, B., et al. (2015). Nonlinear ground vibration identification of an F-16 aircraft - Part 1: Fast nonparametric analysis of distortions in FRF measurements.

[4] Pintelon, R. and Schoukens., J. (2012). *System Identification: A Frequency Domain Approach, second edition*. Piscataway (USA): IEEE Press-Wiley, 2 ed. ISBN 978-0-470-64037-1.

[5] Pintelon, R., Barbé, K., Vandersteen, G., et al. (2011). Improved (non-) parametric identification of dynamic systems excited by periodic signals. *Mechanical Systems and Signal Processing*, 25(7), 2683–2704.

[6] Schoukens, J., Pintelon, R., Rolain, Y., et al. (2001). Frequency response function measurements in the presence of nonlinear distortions. *Automatica*, 37(6), 939–946.

[7] Schoukens, J., Swevers, J., Pintelon, R., et al. (2004). Excitation design for FRF measurements in the presence of non-linear distortions. *Mechanical Systems and Signal Processing*, 18(4), 727–738. ISSN 0888-3270. doi:10.1016/S0888-3270(03)00084-0.

[8] Ertveldt, J., Schoukens, J., Pintelon, R., et al. (2015). Experiments on the Active Aeroelastic Test Bench (AATB) for the Identification of Unsteady Aerodynamics. In *International Forum on Aeroelasticity and Structural Dynamics (IFASD) 2015*. TsAGI.

[9] Ertveldt, J., Pintelon, R., and Vanlanduit, S. (2016). Identification of Unsteady Aerodynamic Forces from Forced Motion Wind Tunnel Experiments. *AIAA Journal*, 54(10), 3265–3273.

[10] Pintelon, R. and Rolain, Y. (2015). Mimo lowly damped system: free-free vibrations of an aluminium tooling plate. In *Proceedings of the 17th IFAC Symposium on System Identification (SYSID 2015)*. Beijing, China, pp. 1466–1470.

[11] Dossogne, T., Nol, J.-P., Grappasonni, C., et al. (2015). Nonlinear ground vibration identification of an F-16 aircraft - Part 2: Understanding Nonlinear Behaviour in Aerospace Structures Using Sine-sweep Testing.

[12] Kerschen, G., Lenaerts, V., and Golinval, J.-C. (2003). VTT benchmark: Application of the restoring force surface method. *Mechanical Systems & Signal Processing*, 17(1). ISSN 0888-3270. doi:10.1006/mssp.2002.1558.

COPYRIGHT STATEMENT